Water Science & Technology

IWA PUBLISHING

Water Science & Technology Vol 87 No 9, 2184 doi: 10.2166/wst.2023.113

Long-term spatial-temporal monitoring of eutrophication in Lake Burdur using remote sensing data

Gizem Tuna Tuygun, Serra Salgut and Alper Elçi*

Department of Environmental Engineering, Dokuz Eylul University, Buca, Izmir 35390, Türkiye
*Corresponding author. E-mail: alper.elci@deu.edu.tr

GTT, 0000-0003-3001-1360; AE, 0000-0002-8102-0438

ABSTRACT

Lake eutrophication continues to be one of the major environmental challenges in lakes worldwide. This study is about using a remote sensing approach to monitor long-term chlorophyll-a (Chl-a) concentrations and the trophic state index (TSI) in Lake Burdur, Türkiye. Surface reflectance from Landsat 5, Landsat 7, and Landsat 8 satellite image collections were evaluated with an empirical equation to estimate a 38-year-long (1984–2021) time series of the lake's median Chl-a concentrations. Pixel quality masking was applied to retain only acceptable quality information and exclude images affected by cloud cover, icing, and other environmental factors from the analysis. The results were analyzed based on annual, seasonal, and monthly temporal averages. Over a period of 38 years, Chl-a concentrations were found to vary between 58.7 and 196.4 mg/m^3. Notably higher concentrations were recorded in 2010 and 2021, while lower concentrations were observed between 1991 and 1993. A substantial increase in Chl-a concentration was evident from 2002 to 2010. The maximum concentration of Chl-a during the first two decades of the analysis was 130 mg/m^3, which increased to 200 mg/m^3 during the last two decades. Landsat-derived TSI values suggested that Lake Burdur has been mostly hypertrophic for the entire study period.

Key words: eutrophication, Landsat, limnology, remote sensing, trophic state

HIGHLIGHTS

- Long-term Chl-a concentration and TSI (trophic state index) monitoring with Google Earth Engine (GEE).
- An increasing trend in Chl-a concentrations was observed for the last 20 years.
- Lake Burdur has been mostly hypertrophic, according to TSI results.
- No significant temporal trend was observed for the entire study period.

GRAPHICAL ABSTRACT

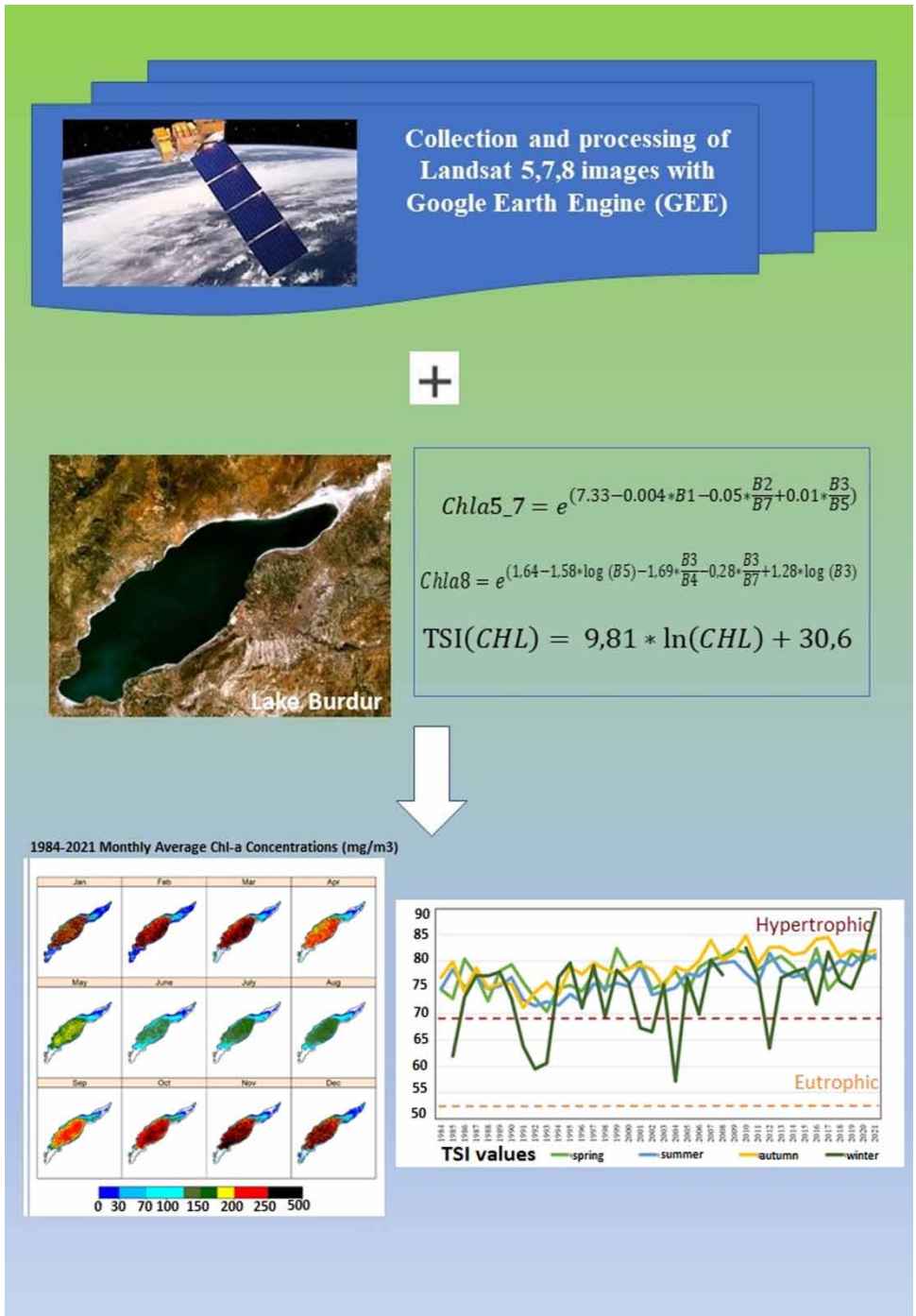

1. INTRODUCTION

Freshwater lakes serve as critical water resources for many areas of the world and have various purposes. However, eutrophication threatens the sustainability of these lakes. Eutrophication trends in lakes are more pronounced in recent decades under the influence of climate change due to increasing anthropogenic pollutant inputs such as ammonium, nitrate, organic nitrogen species, and orthophosphates (Smith 2003; Le *et al.* 2010). Although eutrophication is a natural event of water body enrichment, it can cause significant environmental nuisances and be a problem for water authorities. Long-

term datasets of water quality variables causing lake eutrophication prove useful in developing effective water management strategies (Cao *et al.* 2022).

Traditionally, the water quality of a lake is determined with *in-situ* measurements and laboratory analysis. This approach leads to more or less accurate ground-based measurements that reflect the actual water quality of the lake. However, it requires the allocation of time, monetary and human resources. Furthermore, *in-situ* measurements cannot provide a large-scale spatial and temporal overview of the water quality (Gao *et al.* 2015; Li *et al.* 2017). Lakes in potentially stressed watersheds are frequently ungauged, meaning they are not monitored. Additionally, they may only have a limited number of site measurements that do not provide enough information to assess their level of eutrophication or water quality. In other cases, water quality data may be classified information that is not shared with the public. On the other hand, remote sensing of lakes with satellites offers some possibilities that can be used to estimate water quality variables that are related to eutrophication. It has the benefits of working with a much broader spatial and temporal coverage and being cost-effective and less time-intensive compared with ground measurements. For example, Landsat images have a spatial resolution of 30 m and a revisit cycle of 16 days, while meeting the requirements of image quality and spectral range. The launch of the Landsat-5 Thematic Mapper (TM, 1984–2012), the Landsat-7 Enhanced Thematic Mapper Plus (ETM+, active since 1999), and the Landsat-8 Operational Land Imager (OLI, active since 2013) provided nearly 40 years of satellite imagery, enabling the extraction of historical water quality information (He *et al.* 2021). Landsat images can be used to obtain Chl-a concentrations (Cardall *et al.* 2021; Cao *et al.* 2022), nutrient concentrations (Li *et al.* 2017), transparency or turbidity (Butt & Nazeer 2015; Liu *et al.* 2019), and eutrophication status (Chen *et al.* 2020) in lakes. Among these variables, Chl-a is related to phytoplankton biomass and indicates the lake's trophic status. The trophic state of water bodies can be quantitatively evaluated with the trophic state index (TSI), which was first proposed by Carlson (1977). Several studies for lakes worldwide have shown the potential for TSI to be an effective indicator of lake water quality (e.g., Iwashita *et al.* 2004; Ha *et al.* 2017; Hu *et al.* 2021). It provides a practical lake classification system concerning its trophic state using single or multiple water quality parameters, including either Secchi disk depth, Chl-a concentration, total nitrogen, total phosphorus or as a function of all of them together.

Remote sensing imagery data is widely used to effectively monitor the spatial and temporal dynamics of eutrophication over large areas. In this study, the long-term (1984–2021) and high spatial resolution algae concentrations of Lake Burdur were obtained based on the application of an empirical model on the reflectance time series of Landsat imagery using Google Earth Engine (GEE) (Gorelick *et al.* 2017) as a cloud computing interface. Lake Burdur is under significant environmental stress and the lake's shrinking rate is alarming (Elçi 2019). TSI was also calculated based on Landsat-derived Chl-a concentrations. Inter-annual and seasonal patterns of the TSI and Chl-a concentrations were identified.

2. MATERIAL AND METHODS

2.1. Study area

The Lake Burdur watershed is situated in southwestern Türkiye, between 37.12°–38.17° N and 29.52°–30.85° E as shown in Figure 1, and in a climatic transition zone between the Central Anatolian and Mediterranean regions. The basin is also named the 'Lakes Region' of Türkiye. The long-term mean annual precipitation in the river basin is 444 mm, which is low compared with the typical Mediterranean climate. The largest surface water body is Lake Burdur, which has a declining volume of water with the most recent estimate at 3,900 m^3, and a water surface area of 122.6 km^2 (GDWM 2020). The water surface area of Lake Burdur decreased steadily from 1984 to 2018 (Elçi 2019). The decrease in water levels is due to the construction of upstream dams, increasing water evaporation, and decreasing water inflow to the lake. Lake Burdur is among Türkiye's largest and deepest natural lakes and is located within a closed hydrological basin with a drainage area of 3,211 km^2. The average and the maximum depths are 40 and 100 m, respectively (Girgin *et al.* 2004). Intermittent flowing streams and sporadic groundwater seepage feed the lake. Karstic aquifers in the basin are important water resources that strongly influence the water balances of the lakes.

Organic carbon and nutrient influx originating from diffuse sources, and numerous discharges of industrial and urban wastewater threaten the lake's ecosystem (GDWM 2020). Based on a water quality modeling study by GDWM (2020), the average hydraulic retention time is 33.8 years. This modeling study involved the setup and execution of a basin-scale hydrological model that runs in conjunction with a receiving medium water quality model. In this case, the receiving media was defined as all flowing streams and all lakes in the Burdur Lake watershed. Several scenarios representing actions to improve

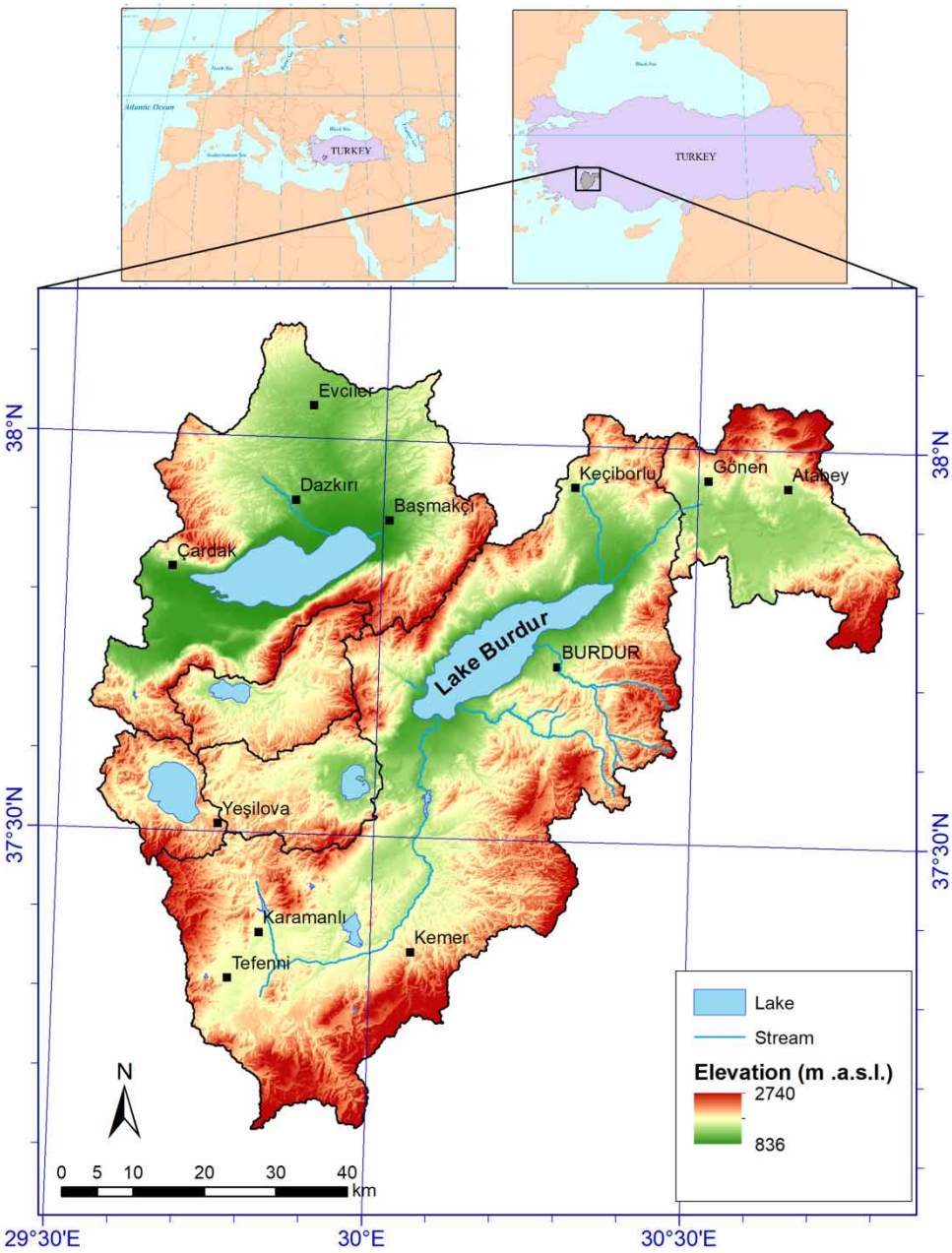

Figure 1 | Location of Lake Burdur in the Lake Burdur watershed in southwestern Türkiye.

water quality and conserve water quantity in the basin were simulated. As a result of the modeling study, changes in lake water volumes, nutrient, priority pollutant, and specific pollutant concentrations were determined, which consequently aided decision-making.

2.2. Data retrieval and processing

This study is executed in three steps: (1) remote sensing data retrieval, (2) remote sensing data pre-processing, and (3) determining spatiotemporal distributions of Chl-a concentrations using the empirical model with Landsat images from 1984 to 2021. The starting date of the study period is defined by the beginning of Landsat data availability, and the ending date marks the end of the calendar year before the time when the study was conducted. Surface reflectance images of Lake Burdur were obtained from the Landsat-5 TM, Landsat-7 ETM + , and Landsat 8 OLI sensors. Landsat data have the longest

records, and the highest consistency spectrum among the current satellites, which makes it suitable for the remote analysis of any surface water quality variable. With the launch of the Landsat-5 Thematic Mapper (TM) in 1984, followed by the Landsat-7 Enhanced Thematic Mapper Plus (ETM+) in 1999 and the Landsat-8 OLI in 2013, nearly 40 years of remote sensing data are available for extracting historical water quality information (Wulder *et al.* 2019; He *et al.* 2021). Although Landsat 5 was decommissioned on 5 June 2013, after 29 years in space and was largely superseded by Landsat 7 and 8 due to equipment failures near the end of their mission, Landsat 7 and Landsat 8 continue to operate. Landsat 5 and 7 have the same band definitions and numbered wavelength ranges in the electromagnetic spectrum, while Landsat 8 has different band definitions. It is important to note that the band names were changed while the Landsat 8 satellite was used. Simultaneously, some cloud computing systems were set up to handle petabytes of geospatial data. GEE is an example of a cloud computing platform that can efficiently provide access, manage, and process big data due to the capabilities of high-performance computing. All data were collected and processed on the GEE platform.

After retrieval of all images for the study period, the data were pre-processed. First, images were cropped to fit the image coverage to the study area, reducing data processing loads. Retrieved images represented data from January 1984 until December 2021 at 16-day intervals. A total of 1,275 images were accessed, although not all images are usable due to cloud, ice, and other issues. GEE commands were used to calculate the Modified Normalized Difference Water Index (MNDWI) (Xu 2006) to mask off the pixels that do not represent water body pixels. Also, pixel quality masking was performed to exclude pixels with issues that affect data accuracy and/or are affected by cloud cover or shadowing. The pixel quality is represented as an integer number stored in a separate band of the Landsat data. After masking, the remaining pixels represent the extent of the visible water body at the time of the image.

In the next step, algae concentrations were computed. Algae concentrations are typically represented as Chl-a concentrations in water. Surface reflectance data from satellite images are used to estimate Chl-a concentrations by using a previously developed empirical model that relates surface reflectance to the unique spectral signature of Chl-a (Hansen & Williams 2018). The empirical model equation developed by Hansen & Williams (2018) was implemented in this study to calculate the Chl-a concentration in each image pixel over the entire 38-year dataset in GEE. This equation represents the empirical relationship between Chl-a and various band surface reflectances from Landsat image data (Equations (1) and (2)). Chl-a spatial distribution maps and time series charts are created with R studio 3.5.2.

The Chl-a equation applied for Landsat 5 and 7 images covering the period 1984–2013:

$$\text{Chla5\_7} = e^{\left(7.33-0.004*B1-0.05*\frac{B2}{B7}+0.01*\frac{B3}{B5}\right)} \tag{1}$$

Similarly, the following Chl-a equation is applied for the Landsat 8 images covering the period 2013–2021:

$$\text{Chla8} = e^{(1.64-1.58*\log(B5)-1.69*\frac{B3}{B4}-0.28*\frac{B3}{B7}+1.28*\log(B3)} \tag{2}$$

where $B1$ is Band 1 (Blue) SR; $B2$ is Band 2 (Green) SR; $B3$ is Band 3 (Red) SR; $B5$ is Band 5 (Short Wavelength Infrared 1) SR; and $B7$ is Band 7 (Short Wavelength Infrared 2) SR.

After applying these equations to each pixel of the bands in an image, Chl-a concentration time series in mg/m^3 are calculated for each pixel. A formal outlier analysis with the IQR (interquartile range) method was performed to identify unusually high Chl-a values that stem from bad-quality image pixels. Consequently, outlier values comprising 16% of all data are excluded from the analysis, which corresponds to roughly a total of six years of data over the 38-year observation period. Finally, by appending the time series obtained from Equations (1) and (2), spatially averaged annual, seasonal, and monthly Chl-a concentrations were calculated to obtain algae concentration time series from 1984 to 2021. Also, the distribution of algae concentrations over the lake is evaluated by computing a median concentration for each month.

Additionally, seasonal TSI values were calculated based on Chl-a concentrations (Equation (3); Carlson 1977). TSI values can be classified into three levels: oligotrophic (TSI < 30), mesotrophic ($30 \leq$ TSI < 50), and eutrophic (TSI ≥ 50). The TSI equation that is related to Chl-a concentration in mg/m^3 was used in this study:

$$\text{TSI(Chl} - \text{a)} = 9.81*\ln(\text{Chl} - \text{a}) + 30.6 \tag{3}$$

3. RESULTS AND DISCUSSION

3.1. Inter-annual variation of Chl-a concentrations and TSI over Lake Burdur

The long-term time series of spatially averaged Chl-a concentrations and corresponding TSI values were obtained for Lake Burdur for 1984–2021, as shown in Figure 2. Chl-a concentrations ranged between 58.7 mg/m^3 (in 1992) and 196.4 mg/m^3 (in 2010). Relatively higher values were observed between 2010 and 2021 and lower values between 1991 and 1993. A significant increase in concentrations was evident for the period 2002–2010. While the maximum Chl-a concentration reached 130 mg/m^3 in the first two decades of the analysis period, it reached 200 mg/m^3 in the recent two decades. Overall, an upward trend in algae concentrations can be observed in the last 20 years, although concentration fluctuates between years.

Figure 2(b) presents the calculated TSI values changing over time. The highest TSI (82.40) was calculated for the year 2010 and the lowest TSI (70.55) for 1992. The TSI value reached 82.40 in 2010, suggesting excessive growth of biomass leading to an algae bloom problem. Overall, the TSI values indicate that Lake Burdur's hypertrophic status from 1984 to 2021 did not change.

There are several possible explanations for the inter-annual variations of Chl-a concentration in Lake Burdur. The lake receives a moderate amount of water from both rainfall and intermittent flowing streams. Since the lake is in a hydrologically closed basin, therefore having no stream outlet, water loss occurs only through evaporation and its hydraulic connection with karstic aquifers. Changes in the difference between precipitation and lake evaporation, as well as a decrease in inflowing stream discharge because of upstream constructions of dams, resulted in a declining lake level (Girgin *et al.* 2004). Furthermore, increasing water demand for agriculture in the lake catchment exacerbates the problem. Davraz *et al.* (2019) conducted a study to evaluate climate and human effects on the hydrology and water quality of Lake Burdur. According to this study, the lake level has been in a state of continuous decline, with a steady shrinking of the lake area. According to this study, 1995 was extremely dry, while moderately dry years were 1986, 1989, 1990, 1992, 1999, and 2008. Conversely, a soaked year was observed in 2003, while moderately wet years were recorded in 1998, 2001, 2009, and 2015. It is worth noting here that the highest Chl-a concentration derived with the remote sensing approach coincides with the aforementioned dry years. It can be concluded from this study that in essence, factors related to the hydrological budget of the lake can directly affect inter-annual variations in Chl-a concentrations and TSI.

3.2. Seasonal variation of Chl-a concentrations and TSI over Lake Burdur

The seasonal changes in the trophic state of Lake Burdur over the past 38 years are shown in Figures 3 and 4. Seasons are defined here as the following: December–February as winter, March–May as spring, June–August as summer, and September–November as autumn. Seasonal dynamics showed visible differences in the study period from 1984 to 2021. Mostly, high Chl-a concentrations were pronounced during autumn and summer. Relatively high concentrations were observed in some years

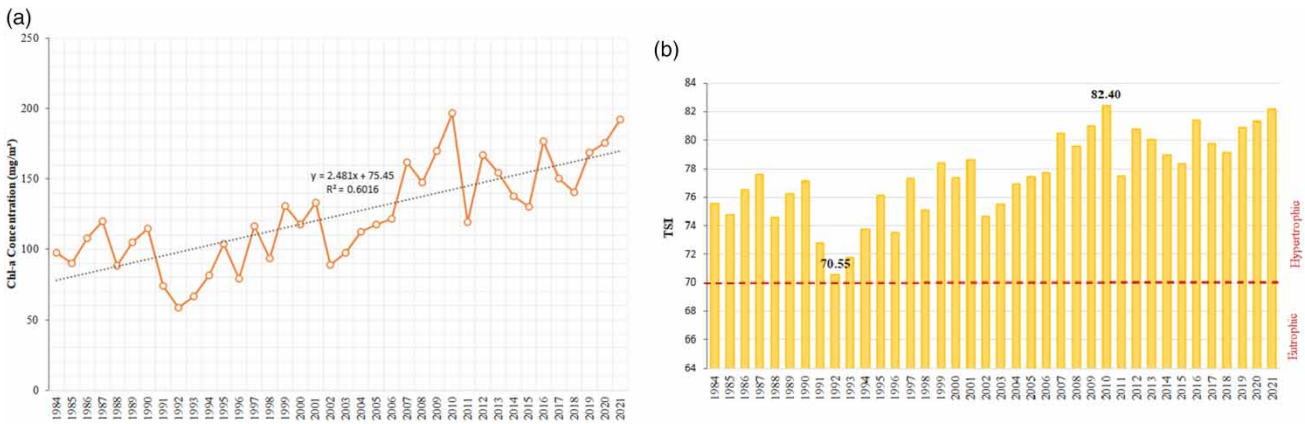

Figure 2 | Inter-annual variation of (a) Chl-a and (b) TSI over Lake Burdur from 1984 to 2021.

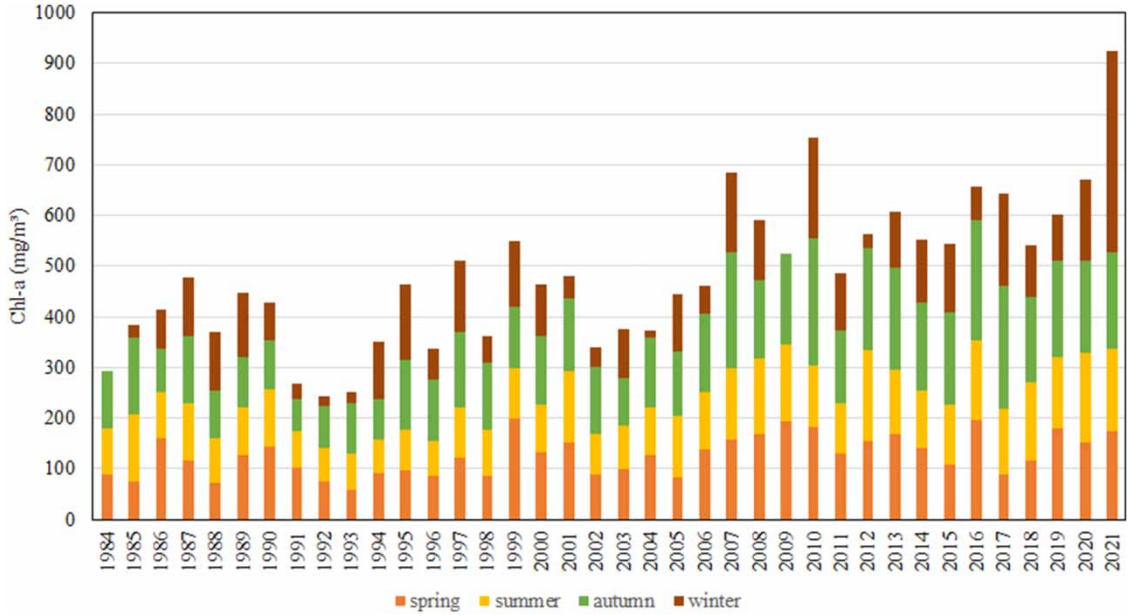

Figure 3 | Seasonal variations of Chl-a concentrations for the period of 1984–2021.

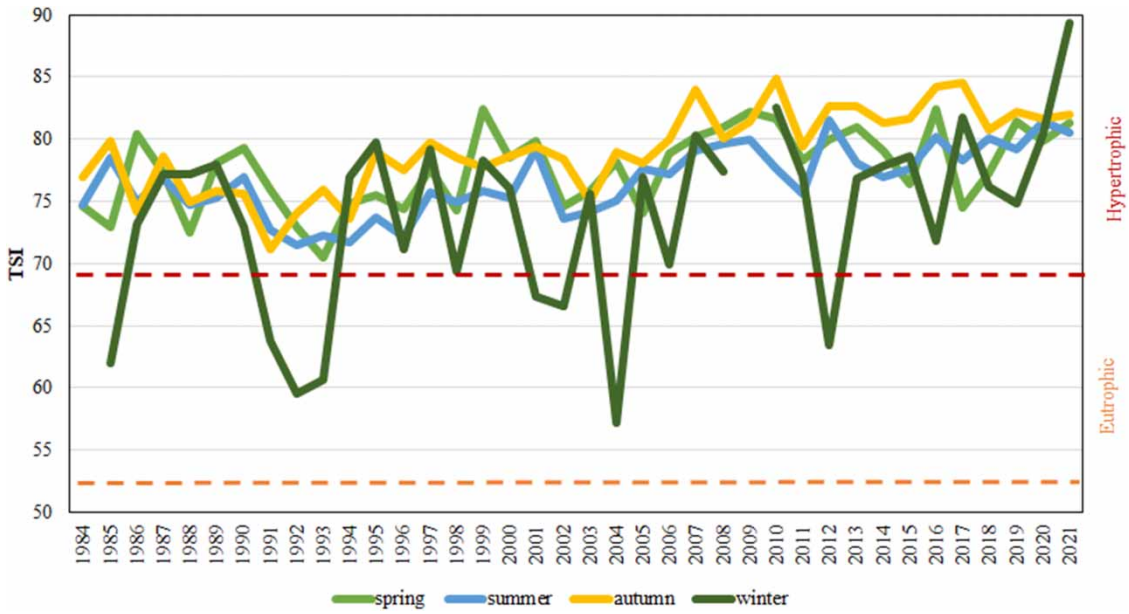

Figure 4 | Seasonal variations of TSI values for the period of 1984–2021.

(e.g., 149 mg/m^3 in the winter of 1997, 252 mg/m^3 in the autumn of 2010, and 397 mg/m^3 in the winter of 2021). Low concentrations were typically seen during spring. However, making a general conclusion about seasonal concentration patterns is difficult. Additionally, the trophic state in winter was more variable than in other seasons. TSI values for spring and summer appeared to be more stable as shown in Figure 4. The lake was mostly hypertrophic, except during the winter months of some years. The TSI showed a seasonal distribution, with the highest average TSI (147.6 $\pm$ 48.1) occurring in autumn and the lowest average TSI (102.8 $\pm$ 69.9) occurring in winter. Spring (126.8 $\pm$ 39.3) and summer (112.9 $\pm$ 31.8) followed autumn, respectively. The standard deviation was highest in the winter and lowest in the summer. The seasonal

patterns remained consistent throughout the study period, indicating that the same factors likely influenced seasonal variations in TSI across the years in this region.

The variability of TSI can be caused by several factors. For example, Girgin *et al.* (2004) found that surface water temperature and salinity were crucial factors affecting the stratification in the lake, hence affecting the hydrodynamics and consequently the distribution and abundance of chlorophyll. Analysis of hydrologic, climatic, and human activity in previous studies suggested that anthropogenic factors were more influential in lake-level changes. In particular, water surpluses originating from high rainfall events in the winter were stored in upstream dams and ponds rather than in Lake Burdur, which led to low water levels and lower TSI values in this season.

Spatial variations of Landsat-derived Chl-a concentrations over the years were also determined to further understand the evolution of Lake Burdur's trophic state. Distribution maps of the multi-annual monthly median Chl-a values from resulting datasets are presented in Figure 5. Temporal variability and fairly stable spatial distribution patterns of Chl-a concentrations could be observed. High and low concentration zones in the lake were consistent for all months. Higher algae concentrations could be seen in the middle of the lake, where the lake is deep. Lower algae concentrations are typically visible in the riverine zones of the lake, where water levels are shallow and water currents more dominant than in other areas of the lake. The temporal rate of Chl-a concentration change appears to be higher in the middle of the lake compared with the nearshore areas. A possible explanation of this observed pattern could be related to differences in lake hydrodynamics, location of point sources along the coastline, and variability of nutrient processing kinetics. More detailed studies would be needed to reach a definite

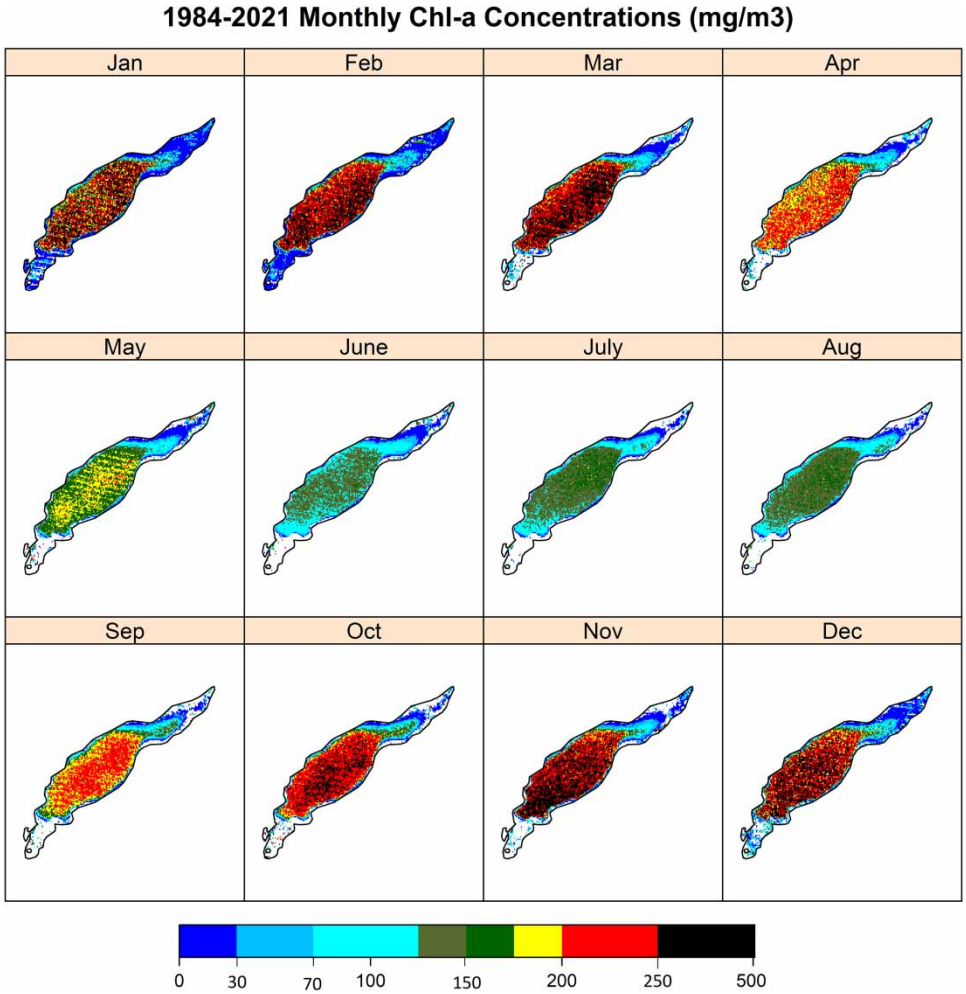

Figure 5 | Spatial distributions of multi-annual monthly median Chl-a concentrations over Lake Burdur.

conclusion. In particular, the dependence of Chl-a concentrations on temporal variations of water depth would be worthwhile to investigate.

Figure 5 also shows that the spatial distribution patterns of temporally averaged Chl-a concentration are similar for all months of the year. Although the Chl-a levels showed absolute differences between different months, the spatial variations displayed a similar pattern. A relatively stable and homogeneous distribution of the highest and lowest values is observed over the lake. Median Chl-a values were highest during October and November, with Chl-a concentrations in the 450–500 mg/m^3 range. Concentrations lower than 200 mg/m^3 could be observed during summer. Overall, it appears that algae blooms in Lake Burdur are typically occurring from November to February and early spring (March) rather than during the late spring (April and May) and summer (June to August), and early fall (September).

3.3. Comparison with *in-situ* measurements

Due to the limited availability of *in-situ* measurement data, it was impossible to validate our results entirely. Nevertheless, the results were compared with the limited amount of measured Chl-a concentration data (Table 1) that was obtained for the years 1997 (Girgin *et al.* 2004) and 2018 (GDWM 2020). All measured Chl-a concentrations reflect Chl-a content in water samples obtained from the water surface of the lake. Error bars for the measured concentration data were not available. Based on the field sampling data, Chl-a concentrations varied between 1.17 mg/m^3 (in October) and 14.74 mg/m^3 (in April) during different months of the 1997 seasons. According to the study, the samples were taken from the surface in the middle of the lake; however, exact sampling coordinates were unknown. The remote sensing monitoring data was consistent with the measured data in April, but significant differences were observed in July and October 1997. Measurements from the GDWM (2020) study provided more comparable results with our Landsat-derived Chl-a concentrations. In 2020, Chl-a concentrations were measured between 291 mg/m^3 (in April) and 750 mg/m^3 (in October). These were in line with spatially averaged estimated concentrations for January, April, and October. However, our results suggested lower Chl-a concentrations for July, unlike the estimated results for the same month in 1997.

Furthermore, it was evident that Chl-a concentrations were lower in 1997. Assuming that measured concentrations are accurate, results from Landsat data overestimated Chl-a levels at the lake surface. It should be noted that considerable uncertainty is included in the *in-situ* data because of timing, location, and method of water sampling. Measurements provided by GDWM (2020) show that Chl-a concentrations were significantly higher in 2018, which was partly confirmed by estimations from Landsat data. It should be noted, however, that estimations given in Table 1 are spatially averaged values and that concentrations over the lake area can vary considerably, as it is shown in Figure 5. A point-by-point comparison of measured and calculated Chl-a concentrations was not possible for two reasons: first, sampling coordinates of the 1997 study were missing. Second, results obtained from Landsat data were available every 16 days, and in some instances, bad-quality pixel clusters that were masked off coincided with the sampling locations.

4. CONCLUSIONS

The novelty of using remote sensing data to determine the long-term trophic state values of lakes is the capability to continuously track and monitor changes over large areas of the lake in time, thereby providing a comprehensive view of the spatial and temporal patterns of eutrophication. As a result, researchers can detect trends and patterns in the lake's trophic state by scrutinizing and contrasting remote sensing data time series pertaining to different time frames. These patterns may consist of

Table 1 | Comparison of Chl-a concentrations with *in-situ* measurements in 1997 and 2018

	Chl-a Concentrations in 1997 (Girgin *et al.* 2004)		Chl-a Concentrations in 2018 (GDWM 2020)	
Months	Measured (mg/m^3)	Estimated monthly range in the present study (mg/m^3)	Measured (mg/m^3)	Estimated monthly range in the present study (mg/m^3)
Jan	–	–	718	66.8–1,567
Apr	14.74	18.8–24.3	291	79.5–219
July	6.82	64.6–135	472	111–199
Oct	1.17	189[a]	750	60.2–933

[a]Only one qualifying data point was available.

surges and downturns in algal blooms as a consequence of alterations in the lake's nutrient concentrations. In this study, long-term satellite remote sensing-based Chl-a concentrations and related TSI index values were obtained for Lake Burdur using empirical equations representing the relationship between optical reflectance and Chl-a concentrations. A procedure was developed using GEE that retrieves raw data, applies the empirical equations to convert information about light reflectances at different wavelengths, and post-process results for interpretation and presentation of the resulting information. Using this procedure, 38 years of reflectance data was processed to determine Chl-a concentrations and explore the spatial-temporal patterns of algae concentrations and the evolution of eutrophication in the lake. The time series of Chl-a concentrations estimated from 1984 to 2021 over Lake Burdur indicated apparent spatial-temporal differences. Spatially, higher Chl-a concentrations were observed in the middle of the lake, possibly associated with factors related to the water depth, and showed a clear decreasing gradient in nearshore regions.

Further studies are needed to investigate the causes of the spatial variability of Chl-a. Anthropogenic organic carbon and nutrient influxes interacting with meteorological factors likely play a key role in the variability of the lake's trophic state. From a seasonal perspective, Chl-a appeared to be higher during the late fall and winter and lower during the summer and spring. Further studies should be conducted to understand the driving factors in particulate climate variables affecting the trophic level by season in the lake. Also, the study can be extended to explore relationships of spatial-temporal trophic state with lake bathymetry, changes in water level, water temperature, point source locations, discharge timings, and the influence of wind and temperature.

The datasets generated in our study provide critical information at a high spatial and temporal resolution, which can be used to identify hotspots of eutrophication and prioritize water management actions. Our research highlights the effectiveness of utilizing multi-Landsat satellite observations in water quality monitoring by expanding the study's temporal and spatial scope. However, due to the lack of an adequate dataset of site measurements, estimated Chl-a concentrations could not be fully validated. Therefore, the estimated concentration values might differ from actual historical concentrations, although the fluctuations and trends are expected to be consistent with actual observations. Conclusively, this non-invasive remote sensing approach can also be applied to other lakes to support strategies for effective watershed management and mitigate problems related to eutrophication.

DATA AVAILABILITY STATEMENT

The data on surface reflectance that was used in this study are openly available in the Earth Engine data catalog at: https://developers.google.com/earth-engine/datasets/catalog/landsat.

CONFLICT OF INTEREST

The authors declare there is no conflict.

REFERENCES

Butt, M. J. & Nazeer, M. 2015 Landsat ETM+ Secchi Disc Transparency (SDT) retrievals for Rawal Lake, Pakistan. *Advances in Space Research* **56** (7), 1428–1440.

Cao, Z., Ma, R., Melack, J. M., Duan, H., Liu, M., Kutser, T., Xue, K., Shen, M., Qi, T. & Yuan, H. 2022 Landsat observations of chlorophyll-a variations in Lake Taihu from 1984 to 2019. *International Journal of Applied Earth Observation and Geoinformation* **106**, 102642.

Cardall, A., Tanner, K. & Gustavious, W. 2021 Google Earth Engine tools for long-term spatiotemporal monitoring of chlorophyll-a concentrations. *Open Water Journal* **7** (1), 1–20.

Carlson, R. E. 1977 A trophic state index for lakes. *Limnology and Oceanography* **22** (2), 361–369.

Chen, Q., Huang, M. & Tang, X. 2020 Eutrophication assessment of seasonal urban lakes in China Yangtze River Basin using Landsat 8-derived Forel-Ule index: A six-year (2013–2018) observation. *Science of the Total Environment* **745**, 135392.

Davraz, A., Sener, E. & Sener, S. 2019 Evaluation of climate and human effects on the hydrology and water quality of Burdur Lake, Turkey. *Journal of African Earth Sciences* **158**, 103569.

Elçi, A., 2019 Analysis of satellite imagery to determine spatial-temporal changes of surface water bodies: A case study of Burdur River Basin, Turkey. In: *Proceedings of the 38th IAHR World Congress. Panama City* (Calvo, L., ed.). IAHR, Panama, pp. 840–845. Available from: https://www.iahr.org/paper/detail?paper_id=2892.

Gao, Y., Gao, J., Yin, H., Liu, C., Xia, T., Wang, J. & Huang, Q. 2015 Remote sensing estimation of the total phosphorus concentration in a large lake using band combinations and regional multivariate statistical modeling techniques. *Journal of Environmental Management* **151**, 33–43.

GDWM 2020 Burdur Nehir Havza Yönetim Planı Nihai Raporu [Final Report of the River Basin Management Plan for Lake Burdur River Basin]. General Directorate of Water Management, Ministry of Agriculture and Forestry, Ankara (in Turkish).

Girgin, S., Kazanci, N. & Dügel, M. 2004 On the limnology of deep and saline Lake Burdur in Turkey. *Acta Hydrochimica et Hydrobiologica* **32** (3), 189–200.

Gorelick, N., Hancher, M., Dixon, M., Ilyushchenko, S., Thau, D. & Moore, R. 2017 Google Earth Engine: Planetary-scale geospatial analysis for everyone. *Remote Sensing of Environment* **202**, 18–27.

Ha, N. T. T., Koike, K., Nhuan, M. T., Canh, B. D., Thao, N. T. P. & Parsons, M. 2017 Landsat 8/OLI Two bands ratio algorithm for chlorophyll-a concentration mapping in hypertrophic waters: An application to west lake in Hanoi (Vietnam). *IEEE Journal of Selected Topics in Applied Earth Observations and Remote Sensing* **10** (11), 4919–4929.

Hansen, C. H. & Williams, G. P. 2018 Evaluating remote sensing model specification methods for estimating water quality in optically diverse lakes throughout the growing season. *Hydrology* **5** (4), 62.

He, T., Xiao, W., Zhao, Y., Chen, W., Deng, X. & Zhang, J. 2021 Continues monitoring of subsidence water in mining area from the eastern plain in China from 1986 to 2018 using Landsat imagery and Google Earth Engine. *Journal of Cleaner Production* **279**, 123610.

Hu, M., Ma, R., Cao, Z., Xiong, J. & Xue, K. 2021 Remote estimation of trophic state index for inland waters using Landsat-8 OLI imagery. *Remote Sensing* **13** (10), 1988.

Iwashita, K., Kudoh, K., Fujii, H. & Nishikawa, H. 2004 Satellite analysis for water flow of Lake Inbanuma. *Advances in Space Research* **33** (3), 284–289.

Le, C., Zha, Y., Li, Y., Sun, D., Lu, H. & Yin, B. 2010 Eutrophication of lake waters in China: Cost, causes, and control. *Environmental Management* **45** (4), 662–668.

Li, Y., Zhang, Y., Shi, K., Zhu, G., Zhou, Y., Zhang, Y. & Guo, Y. 2017 Monitoring spatiotemporal variations in nutrients in a large drinking water reservoir and their relationships with hydrological and meteorological conditions based on Landsat 8 imagery. *Science of the Total Environment* **599–600**, 1705–1717.

Liu, D., Duan, H., Yu, S., Shen, M. & Xue, K. 2019 Human-induced eutrophication dominates the bio-optical compositions of suspended particles in shallow lakes: implications for remote sensing. *Science of The Total Environment* **667**, 112–123.

Smith, V. H. 2003 Eutrophication of freshwater and coastal marine ecosystems: A global problem. *Environmental Science and Pollution Research* **10** (2), 126–139.

Wulder, M. A., Loveland, T. R., Roy, D. P., Crawford, C. J., Masek, J. G., Woodcock, C. E., Allen, R. G., Anderson, M. C., Belward, A. S., Cohen, W. B., Dwyer, J., Erb, A., Gao, F., Griffiths, P., Helder, D., Hermosilla, T., Hipple, J. D., Hostert, P., Hughes, M. J., Huntington, J., Johnson, D. M., Kennedy, R., Kilic, A., Li, Z., Lymburner, L., McCorkel, J., Pahlevan, N., Scambos, T. A., Schaaf, C., Schott, J. R., Sheng, Y., Storey, J., Vermote, E., Vogelmann, J., White, J. C., Wynne, R. H. & Zhu, Z. 2019 Current status of Landsat program, science, and applications. *Remote Sensing of Environment* **225**, 127–147.

Xu, H. 2006 Modification of normalised difference water index (NDWI) to enhance open water features in remotely sensed imagery. *International Journal of Remote Sensing* **27** (14), 3025–3033.

First received 24 November 2022; accepted in revised form 3 April 2023. Available online 13 April 2023